

Investigations of Polyacrylamide Nanofibres as Probable Adsorbents for CO₂ Capture

K. A. Oyewole^{a*}, G. T. Vladislavjevic^b and B. Benyahia^b

^aDepartment of Chemical Engineering, Osun State University, Osogbo, Nigeria

^bDepartment of Chemical Engineering, Loughborough University, Loughborough, UK

*Corresponding Author: kehindefayemiwo@uniosun.edu.ng

ARTICLE INFO

Received: January, 2022

Accepted: April, 2022

Published: April, 2022

Keywords:

Adsorbents

Electrospinning

Nanofibres

Polyacrylamide.

ABSTRACT

Polyacrylamide was synthesised via bulk polymerisation of acrylamide using azobisisobutyronitrile and acetonitrile as initiator and porogenic solvent respectively. The polyacrylamide was electrospun to produce polyacrylamide nanofibres (PAmNF). The influence of the concentration of the polymer, flow rate, the voltage applied and tip-to-collector distance ratio on the fibres morphology and diameters were studied to determine the best electrospinning conditions. The nitrogen adsorption-desorption isotherms at 77 K were used to evaluate the surface characteristics of the nanofibre. The nanofibre was found to exhibit an average pore size, total pore volume and Brunauer-Emmett-Teller surface area (S_{BET}) up to 12 nm, 0.06 cm³ g⁻¹ and 26 m² g⁻¹, respectively. The CO₂ and N₂ sorption uptake of the nanofibre was also investigated at 273 K. The nanofibre has a low affinity for CO₂ (0.08 mmol/g at 1 bar). This could have been because of the absence of cross-linking agents, thus establishing the importance of crosslinkers in the synthesis of polymers for CO₂ capture. Also, another likely possible solution to enhance the CO₂ uptake could have been by carbonisation of the electrospun fibres at high temperatures.

1. INTRODUCTION

Carbon dioxide emission during the combustion of fossil fuels has been identified as one of the major causes of climate change and global warming (Oyewole *et al.*, 2023; Fayemiwo *et al.*, 2019). There is a continuous growth in energy demand and several efforts have been geared toward alternative energy development, nonetheless, it is very unlikely that dependence on fossil fuels will reduce in the nearest future (Fayemiwo *et al.*, 2018). It is therefore essential to seek possible technologies to capture CO₂ to lower its emission into the atmosphere and mitigate its environmental effect (Mac Dowell *et al.*, 2017). Researchers are thereby prompted to develop materials that are adept to capture CO₂ for the purpose of alleviating this parasitic load (Gur, 2022; Fayemiwo *et al.*, 2017).

Over recent decades, there is a significant growing interest in the prospective application of electrospinning of polymers to produce polymer nanofibres with a wide range of complex structures of nanofibres and nonwovens (Dos-Santos *et al.*, 2020; Xue *et al.*, 2017; Feng *et al.*, 2010). Electrospinning has grown to become a novel and preferred method to fabricate nanoscale fibres from polymer solutions (Bhardwaj, 2010). By virtue of their large surface areas, ease of regeneration, thermal stabilities and chemical resistances, electrospun nanofibres have been considered potential adsorbents (Min *et al.*, 2016; Lee *et al.*, 2010). Nanofibres have been widely used in a number of applications such as tissue engineering (Malik *et*

al., 2021; Kumar *et al.*, 2018), drugs release (Abdul Hameed *et al.*, 2023; Contreras-Cáceres *et al.*, 2019), chemical and optical sensors (Schoolaert *et al.*, 2017; Long *et al.*, 2012). More recently, they have also been applied in CO₂ capture (Ouyang *et al.*, 2018; Li *et al.*, 2016).

In a recent report, electrospun nanofibres functionalised with a metal-organic framework (MOF) were fabricated using polyacrylonitrile (PAN) as a precursor polymer (Wahiduzzaman *et al.*, 2015). It was observed that the adsorbent gave 13.76% and 6.03% reduction in CO₂ concentration at an outlet in the first and second cycle respectively. In another work, chemically activated N-doped carbon nanofibres were synthesised for CO₂ capture adsorbents using pyrrole monomer as a starting precursor (Li *et al.*, 2016). It was reported that the CO₂ capture capacities measured for the un-activated carbons nanofibres are found to be very low, notwithstanding the temperature at which carbonisation was carried out. Iqbal *et al.* (2017) also reported the production of nanofibres integrated with amine-functionalised carbon nanotubes using polyacrylonitrile (PAN) as a precursor. The nanofibres produced were carbonised at 850 °C and reported to have Brunauer-Emmett-Teller surface area (S_{BET}) up to 427 m²/g and CO₂ uptake of 6.3 mmol/g at 1.0 bar and 298 K. It was believed that the carbon nanotubes introduced added strength to the adsorbents and prevented cracking.

In this work, polyacrylamide nanofibres were fabricated through the electrospinning process. The conditions of the electrospinning were varied under four major variables, tip-to-collector distance (TCD), applied voltage, feed flow rate and feed solution concentration. The gas sorption characteristic were also investigated and reported accordingly. The feasibility of polyacrylamide nanofibres as potential adsorbents for CO₂ capture was also investigated.

2. METHODOLOGY

2.1 Materials

Fisher Scientific in the United Kingdom supplied acetonitrile (ACN). Sigma Aldrich, UK, provided the monomer acrylamide (AAM) and the initiator azobisisobutyronitrile (AIBN) used in the polymer synthesis. Analytical-grade reagents were used throughout. Pure water was supplied using a Millipore Milli-Q Plus 185 water filtration system. BOC, UK, supplied all of the gases with a purity of more than 99.99%.

2.2 Polymer Synthesis

At the start, ACN was used to dissolve the monomer (AAM) and initiator (AIBN). In order to get rid of the dissolved oxygen, the resulting mixture was then purged for 10 minutes using nitrogen gas and sealed afterwards. For polymerisation, it was placed in a water bath set at 60 °C for 24 hours. After polymerisation, the monolithic polymer was crushed and ground. It was then rinsed in methanol to get rid of any unreacted monomer and then filtered. The polymer was placed in a vacuum oven set at 80 °C and allowed to dry overnight.

2.3 Feed Solution Preparation

The polymer (12-18 wt.%) synthesis was completely dissolved in distilled water at 40 °C. The solution of the polymer viscosities is within the range of 0.20 Pa.s $\leq \mu \leq$ 0.40 Pa.s, with conductivities \leq 1480 mS. The solution was loaded into a 10 ml plastic syringe for each sample fabricated (Table 1).

2.4 Electrospinning

The electrospinning device used was fabricated at the Chemical Engineering Research Centre. Figure 1 showed the schematic set-up of the device, the loaded syringe was fixed into the spinneret. As the voltage was applied, the solution of the polymer was stretched electrostatically after being injected at a steady flow rate through a syringe placed horizontally. A flat plate wrapped with an aluminium foil set at a predetermined distance from the needle tip was used to collect the fibres. The conditions of the

electrospinning are as stated in Table 1, samples were conducted in triplicate for analysis of the best condition.

Table 1: Different Parameters used for the Electrospinning*

Sample	Solvent volume (ml)	Feed conc. (%)	Applied voltage (kV)	Feed rate (ml/h)	TCD (cm)	\bar{d} nm	σ	CV %
PAmNF-1	120	18	25	1	7.5	64	20	31
PAmNF-2	120	18	25	1	10	45	17	38
PAmNF-3	120	18	25	1	12	80	18	23
PAmNF-4	120	18	25	1	15	76	18	24
PAmNF-5	120	18	25	0.5	10	72	15	21
PAmNF-6	120	18	25	2	10	64	10	16
PAmNF-7	120	18	15	1	10	61	19	31
PAmNF-8	120	18	20	1	10	76	28	37
PAmNF-9	120	12	25	1	10	33	17	52
PAmNF-10	120	15	25	1	10	29	9	31

*Feed solution concentration is in % wt./vol., \bar{d} is the average nanofibre diameter, σ is the standard deviation and CV is the coefficient of variation.

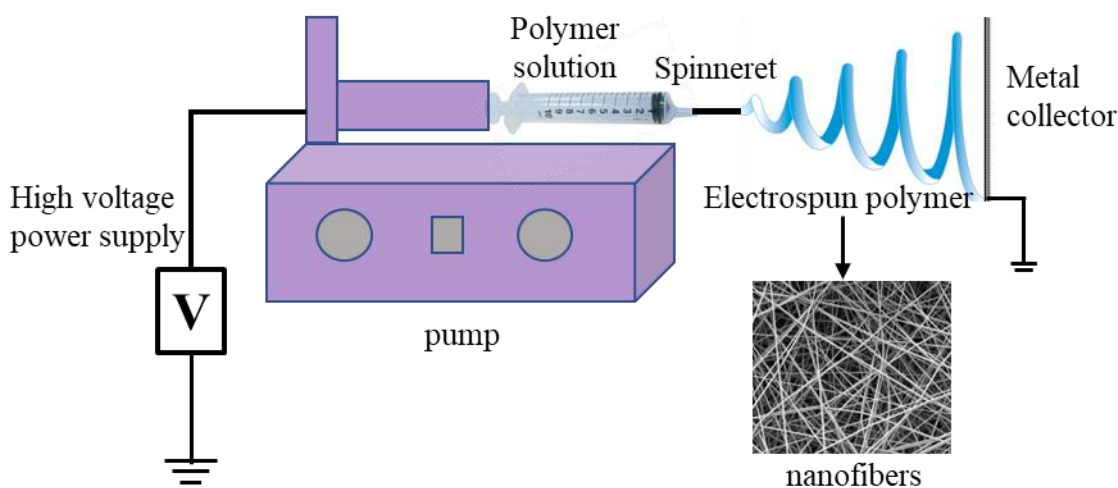


Figure 1: Schematic Diagram of the Electrospinning Process

2.5 Fibres Characterisation

Scanning electron microscope (SEM) Zeiss 1530 VP FEG-SEM operating at an accelerating voltage of 5 kV, working distance of 14 mm and a magnification of x 75,000 was used to investigate the morphology of the electrospun nanofibre samples. Prior to each scanning, gold/palladium alloy was used to coat the electrospun nanofibre samples using a benchtop sputter/coater, Quorum Q150R S for 60 s. This was done in order to increase the samples' conductivity and minimize the build-up of electrostatic charges that might result in a charging effect on the nanofibres during imaging. The SEM images were studied using the image processing software, 'ImageJ'.

On each SEM image, the nanofibre diameters were measured, and the minimum, maximum, mean and standard deviation of the fibres were evaluated. The measurements were plotted and the size distribution of nanofibres in each sample was obtained. Also, the coefficient of variation (CV), a relative measure of the variation of fibre diameters from the mean of the data set was calculated. The midpoint (d_{mi}) of each size range was calculated from Equation 1 and the average mean diameter (\bar{d}) was calculated using Equation 2. Where d_{min} and d_{max} is the minimum and maximum diameter (nm) respectively. The standard deviation and coefficient of variation were determined from Equations 3 and 4 respectively. Where f is the frequency and σ is the standard deviation.

$$d_{mi} = \frac{d_{max,i} + d_{min,i}}{2} \quad (1)$$

$$\bar{d} = \frac{\sum f_i d_{mi}}{\sum f_i} \quad (2)$$

$$\sigma = \sqrt{\frac{\sum f_i (d_{mi} - \bar{d})^2}{\sum f_i}} \quad (3)$$

$$CV = \frac{\sigma}{\bar{d}} \quad (4)$$

3. RESULTS AND DISCUSSION

3.1 Tip-to-Collector Distance (TCD) Effect

The quality and diameter of fibres collected are mainly affected by two factors, the flight time and the electrical field strength of the fibre (Bhardwaj and Kundu, 2010; Thompson *et al.*, 2007). Since the electrical field strength is inversely related to TCD, the apparent field strength that draws out the fibres decreases as the distance increases. As a result of being stretched by a weaker electric field, fibres gathered at a higher TCD are expected to have a larger diameter (Bhardwaj and Kundu, 2010). The results obtained for average nanofibre diameter values support this theory (Table 1), as evidenced by the samples obtained at further TCDs (12 cm and 15 cm); PAmNF-3 and PAmNF-4 have the highest diameters in the sample set, measuring 80 nm and 76 nm, respectively.

Moreover, as a longer distance necessitates a greater time for the nanofibre to reach the collector, the nanofibres' flight duration is directly correlated to the TCD (He *et al.*, 2021). The electric field can whip and stretch the fibres to a larger extent at this moment. The fibres could evaporate as the flight times get longer, resulting in fewer fused fibres on the collector plate. There is no correlation between TCD values and average fibre diameters. This is explained by the trade-off between greater flight time and decreasing field strength as TCD increases. Furthermore, the TCD has no significant influence on the standard deviation, with values ranging from 18 to 20, and the variation coefficient, with values ranging from 23% to 31%, indicating that there is no effect on the homogeneity of the nanofibres.

The SEM image in Figure 2 also revealed that more fusion occurred within fibres with a low TCD (PAmNF-1 and PAmNF-2), which was likely due to their short flight times and incapability to fully evaporate. When the magnification is higher, as shown in Figure 2, it was revealed that the majority of the fibres in PAmNF-1, which had the lowest TCD value of 7.5 cm, had severe damage, while PAmNF-2 also had evidence of

damage, albeit to a lesser level. PAmNF-4 at 15 cm exhibits considerable fibre breakage, however, when compared with those collected at a lower TCD, the breakage is significantly lesser. PAmNF-3 spun at 12 cm reveals excellent high-quality fibres and denotes the almost ideal distance for TCD. Samples PAmNF-1, PAmNF-2, and PAmNF-4 all exhibit significant bead development when viewed at lower magnifications, however, PAmNF-3 contained relatively few beads. There is, however, no conclusive proof that the formation of beads and TCD are related.

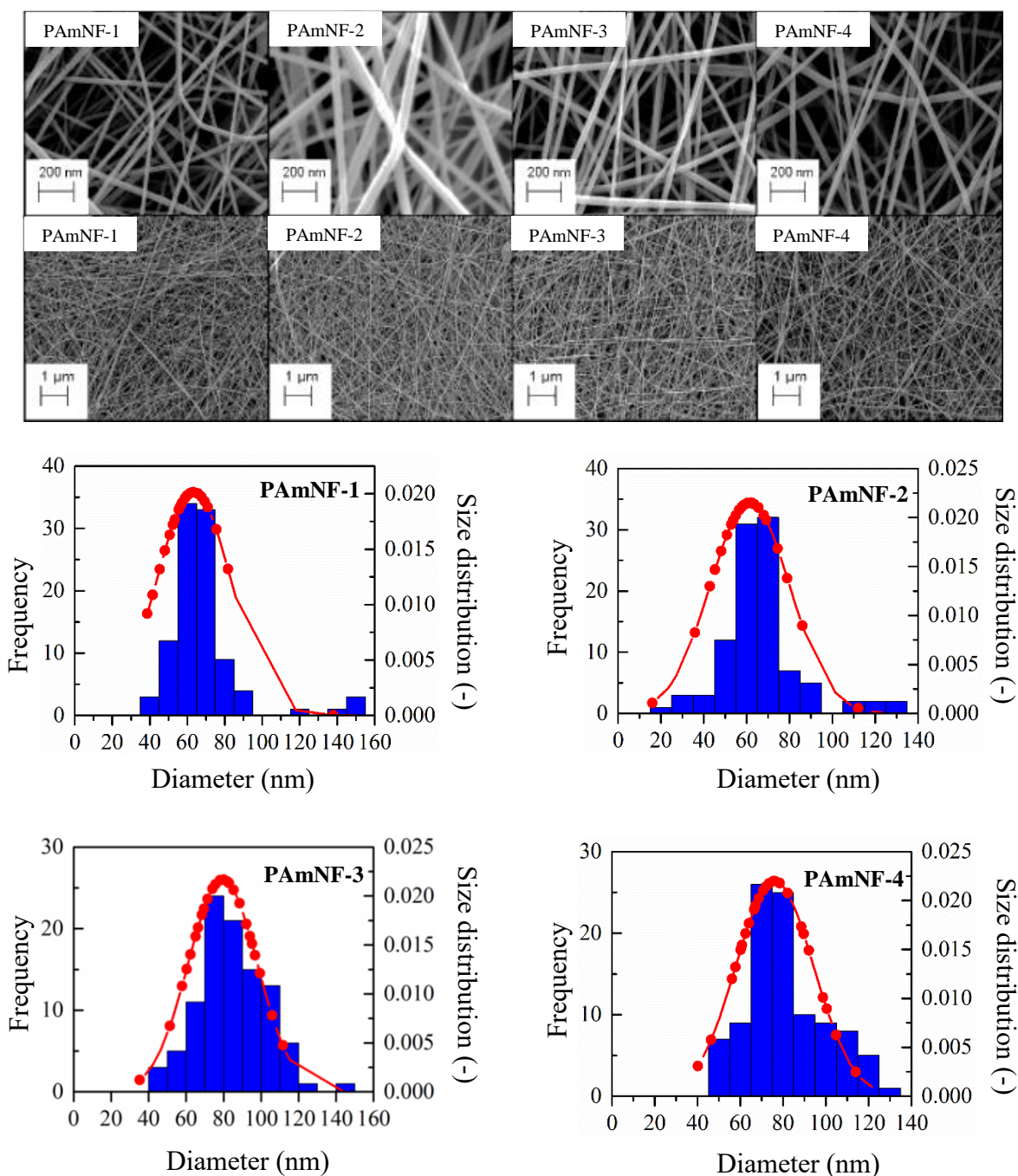


Figure 2: Effect of tip-to-collector distance (TCD) on the morphology scanning electron micrographs of the PAmNF with nanofibres diameter distribution as produced from solutions of 18 % (w/v) of polyacrylamide at 25 kV and 1 ml/h.

3.2 Effect of Feed Flow Rate

All other variables were held constant, three different feed flow rates were investigated to study their impact on the morphology of the fibres. Sample PAmNF-5 electrospun at the lowest feed flow rate (0.5 ml/h) exhibited the highest nanofibre average diameter of 72 nm (Table 1). The frequency distribution in Figure 3 shows more proof of this that a greater percentage of the sample's nanofibres were concentrated around larger diameters of nanofibres between 65-95 nm. This feed flow rate ought to be ideal, according to theory, because it allows the solvent more time to evaporate and generate solid nanofibres. On the contrary, the SEM image of nanofibres in sample PAmNF-5 in Figure 3 shows that the nanofibres are extremely small and have several breakages throughout their length.

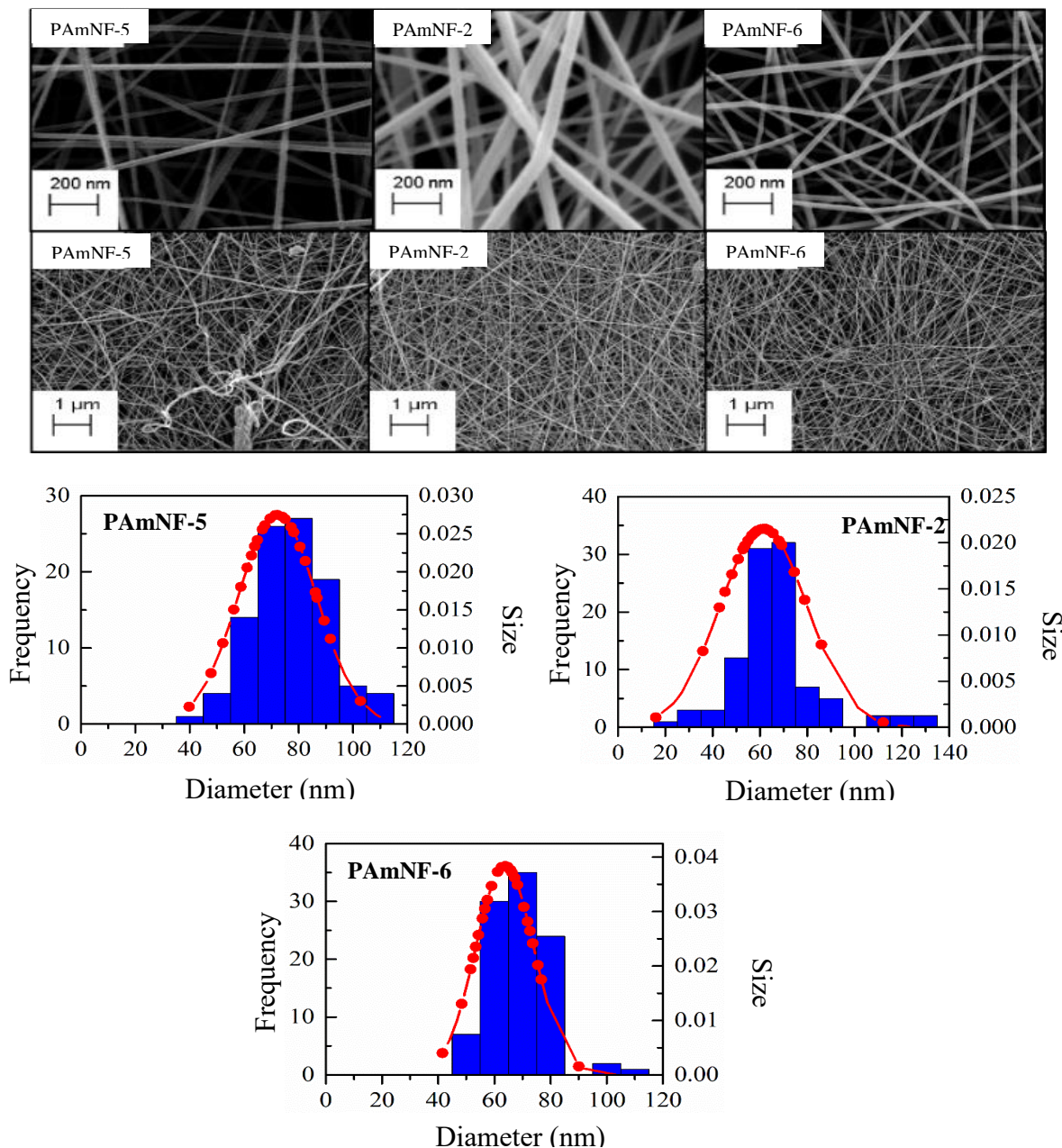


Figure 3: Effect of feed flow rate on the morphology scanning electron micrographs of the PAmNF with nanofibres diameter distribution as produced from solutions of 18 % (w/v) of polyacrylamide at 25 kV and 10 cm.

This is due to the fact that the pace at which the polymer solution is fed into the needle's tip is too slow to keep up with the rate at which it is being removed from the tip, which inhibits the electrospinning process. Furthermore, this is demonstrated by the presence of considerable deformation in the electrospun nanofibre generated when droplets of polymer solution were not stretched sufficiently. When PAmNF-6 was spun at the greatest feed flow rate of 2 ml/hr, the development of beaded nanofibres was more favoured, resulting in thick, average diameters of 64 nm (Table 1). This is due to both the modest stretching forces of the applied voltage and the short solvent evaporation time before the fibres reach the collecting plate. Despite the fact that all of the samples in this set were electrospun at 25 kV, the high rate at which droplets were generated at the tip of the needle overcame its impact on stretching the droplets of the polymer solution. The excessive nanofibre thinning generated by the high flow rate (2 ml/h) and high applied voltage (25 kV) led to the development of weaker nanofibres that were more prone to breaking, as can be seen in the SEM image of PAmNF-6 in Figure 3.

The smoothest nanofibres with the narrowest diameters of 45 nm were created at a feed rate of 1 ml/h (PAmNF-2) due to the minimum solvent evaporation time before reaching the collector plate, resulting in fewer beads. The CV values in this sample set differ significantly, demonstrating that the feed flow rate has a significant impact on the consistency of the nanofibre sizes. PAmNF-6 has the lowest CV value (16%), indicating that it has the most consistent distribution of nanofibre diameters in the sample set, despite the presence of beads. When subjected to gaseous flow, the presence of the beads might induce a channelling effect because the size of the pore spaces changes.

3.3 Effect of Applied Voltage

Smooth and uniform nanofibres with an average diameter of 61 nm were produced with minimum beads formation at a low voltage of 15 kV (PAmNF-7). The applied voltage was able to create an electrostatic force strong enough to overcome viscoelastic forces while also twisting the droplet of polymer solution, causing it to stretch into a uniform nanofibre as a result of the electrospinning process. At 20 kV and above, more charges flow from the needle tip due and tend to become non-stable, resulting in a distinct form of droplet breakdown. As seen in Figure 4, this resulted in the development of non-uniform nanofibres that are more prone to breakage. Moreover, high voltages cause beads formation as voltage increases leading to the rate of solution delivery to the needle tip must be greater than the rate of solution evaporation from the needle tip in order to keep the nanofibres' cylindrical shape. As a result, droplets that developed at the needle's tip are taken away before they can stretch into fibres. With a low CV value of 31% compared to PAmNF-8 and PAmNF-2 at 37% and 38%, respectively, sample PAmNF-7 has the most consistent nanofibre diameters in the sample set, as can be seen from the SEM images of PAmNF-7 to PAmNF-8 in Figure 4. As there are still beaded nanofibres present, PAmNF-7 is the best option among the other samples in the collection for use as a filter medium for CO₂ capture.

3.4 Effect Polymer Solution Concentration

As the concentration of the polymer is increased, the polymer solution viscosity increases and the nanofibres are getting thicker with noticeable differences in their SEM morphology, PAmNF-9 < PAmNF-10 < PAmNF-2 (Figure 5). PAmNF-9 fabricated from 12 % wt./vol. show up to have the thinnest nanofibres, while PAmNF-2 electrospun from 18 % wt./vol. yielded the thickest nanofibres. It is revealed that as the polymer concentration grows, the quality of the nanofibres improves while the number of beads within decreases, indicating that high viscosity promotes the development of nanofibres. At higher magnification, all of the samples had breakages and cracks on the fibres, as seen in the SEM pictures in Figure 5. However, as feed polymer concentration rises, the fibres grow smoother. In addition, the beads on the fibres are spaced more apart on average. In PAmNF-9, the beaded nanofibres are more closely packed, with beads appearing on each fibre about every 0.7 nm. As the concentration and viscosity of the polymer solutions rise, the samples become less densely populated.

The high CV value of 52% of sample PAmNF-9 proves that low feed solution concentrations lead to the formation of very low-quality nanofibres with beads, which causes a negative effect on the consistency of the nanofibre diameters. Although sample PAmNF-10 had thin nanofibres with beads, it had the lowest CV value in the sample set of 31%. A low feed solution concentration results in the development of very poor-quality nanofibres with beads, which has a severe impact on the uniformity of the nanofibre diameters, as shown by the high CV value of 52% of sample PAmNF-9. Despite having thin nanofibres with beads, sample PAmNF-10 showed the lowest CV value in the sample set (31%). When thinking about a nanofibre sample as a filter medium for carbon capture, lower CV values are preferable.

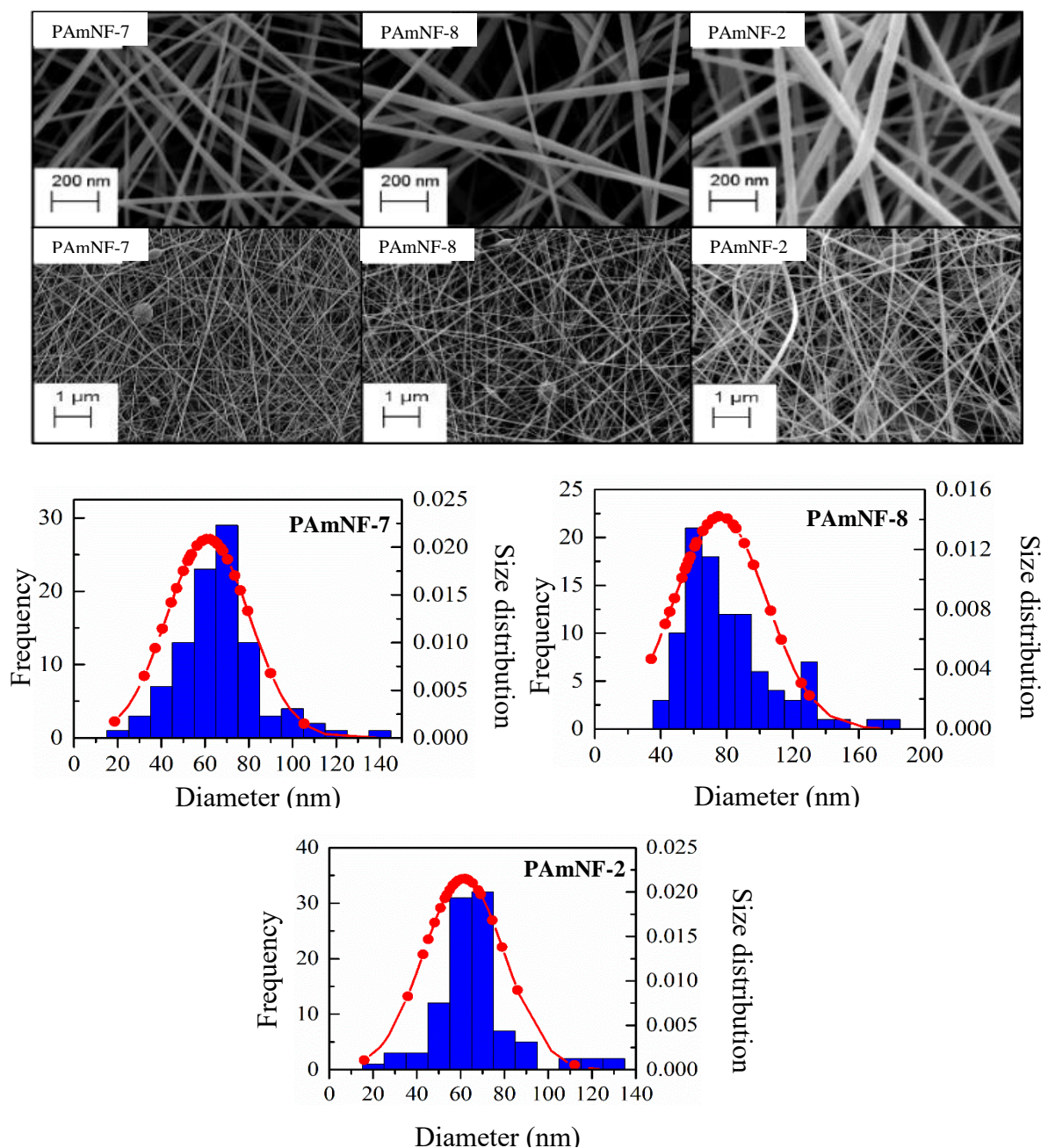


Figure 4: Effect of applied voltage on the morphology scanning electron micrographs of the PANF with nanofibres diameter distribution as produced from solutions of 18 % (w/v) of polyacrylamide at 1 ml/h and 10 cm.

Sample PAmNF-2 appears to be the best, if not the greatest, because it still contains beads, but fewer beads than the other samples in the collection. PAmNF-2 had the thickest nanofibres, which was not necessarily optimal, but it also had a CV value of 38%, which was greater than PAmNF-10's CV value. Its use as a carbon capture filter media would likely outperform that of PAmNF-10 since it compensates for a larger diameter with fewer beads and vice versa. Finally, the concentration of the feed solution has a significant impact on both the regularity of the diameter distribution and the presence of beads. To completely eliminate the presence of beads and produce smoother nanofibres, a greater feed solution concentration could be used to attain an optimal nanofibre morphology.

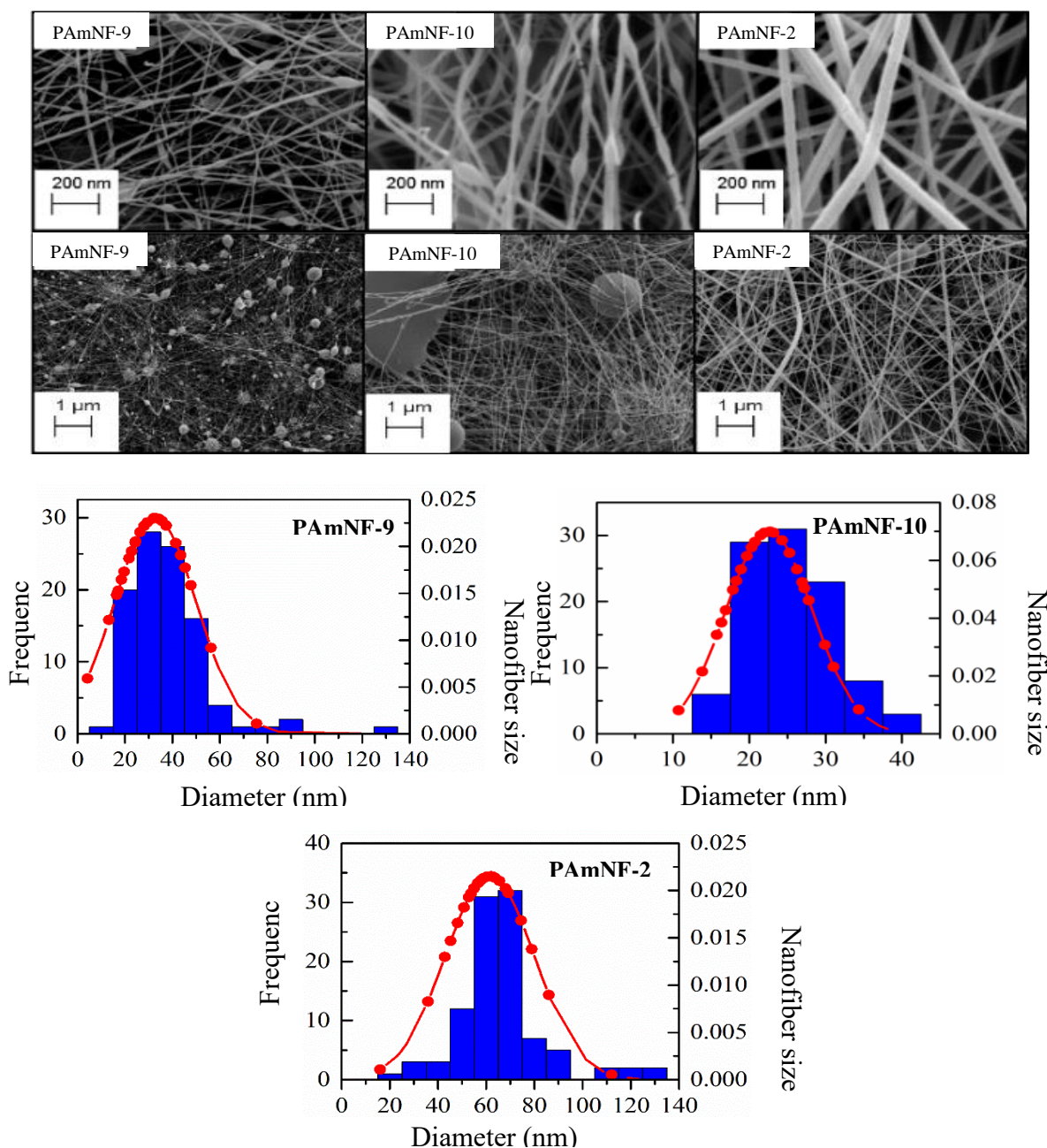


Figure 5: Effect of polymer concentration on the morphology scanning electron micrographs of the PAmNF with nanofibres diameter distribution as produced from solutions of 12 %, 15 % and 18 % (w/v) of polyacrylamide at 25 kV, 1 ml/h and 10 cm TCD.

3.5 Investigation of Gas Sorption

As evidenced in the nitrogen adsorption-desorption isotherms of one of the samples evaluated at 77 K (Figure 6), the PAFN displayed Type II isotherms according to the IUPAC classification (Sing, 1985). Below P/P_0 of 0.1, monolayer coverage was completed, followed by multilayer adsorption at a higher value. The CO_2/N_2 uptake was assessed at 273 K and shown in Figure 7. Although, the gas materials selectively adsorbed CO_2 as compared to the N_2 , however, the adsorption performance was very poor (0.08 mmol/g); thus, the nanofibre has a low affinity for CO_2 . One likely reason for this could have been because of the absence of a crosslinker in the synthesis of the polymer. It's worth noting that this was the first attempt, therefore further effort would be made to investigate the likely way forward to achieve higher CO_2 capture with nanofibres.

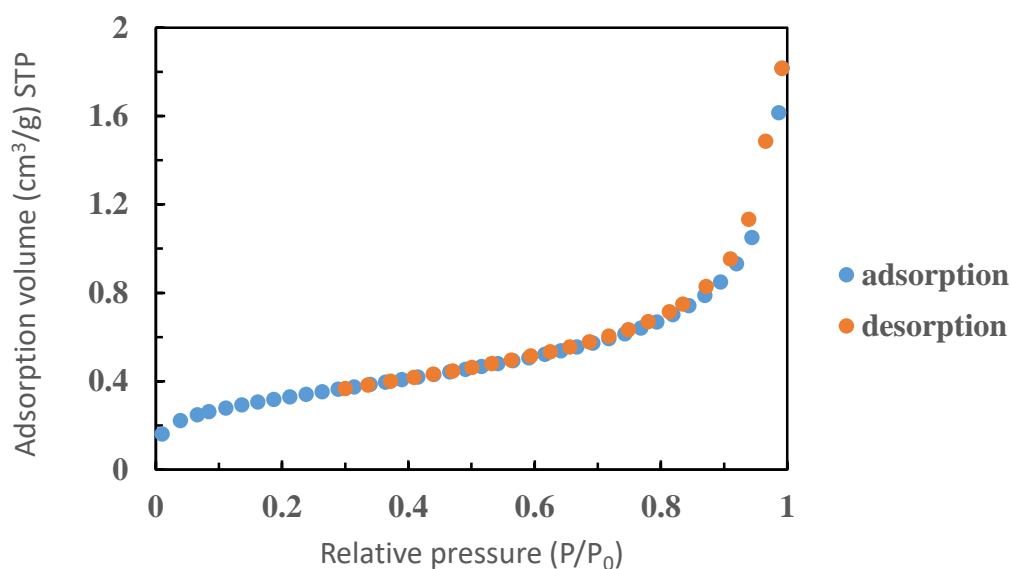


Figure 6: Nitrogen adsorption-desorption isotherms of PAmNF-2 investigated at 77 K. The sample follows Type II isotherms.

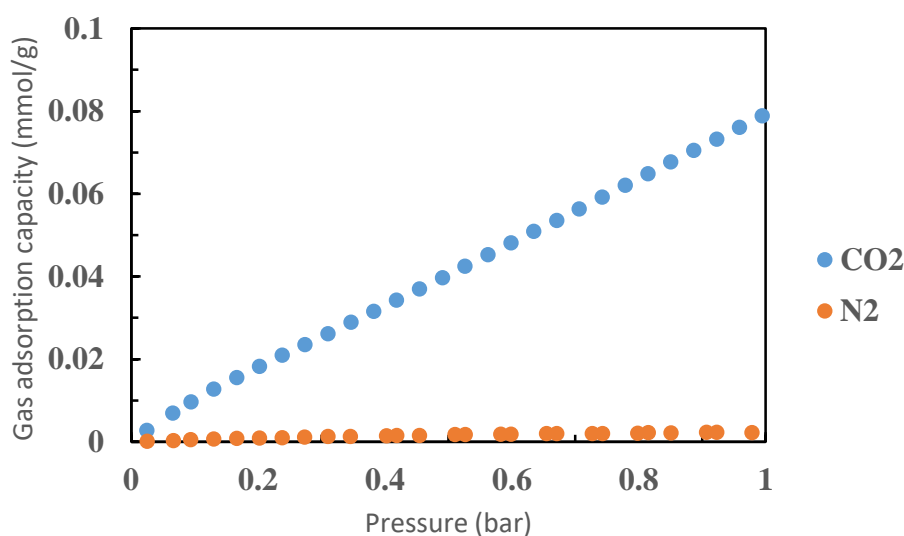


Figure 7: The CO_2 and N_2 adsorption isotherms of the PAmNF-2 investigated at 273 K

4. CONCLUSION

Here, an attempt was made to produce polyacrylamide nanofibres (PAmNF) for CO₂ capture. This would be the first time attempting to fabricate nanofibres for CO₂ capture from the bases of first synthesising the polymer from monomer, as other works reported so far made use of polymers directly. Although, the nanofibres synthesised had low affinity for CO₂, however, it is worth investigating the likely reasons and doing further research on how to achieve the goal of high CO₂ affinity poly-nanofibres. When the electrospinning operating conditions and parameters were probed, high feed solution (up to 18 %) played a major role in enhancing the quality of the fibres produced, due to higher viscosity which also led to lower beads formation within the nanofibres. When the TCD was increased above 12 cm, significant fibres damage occurred, while a feed flow rate of 0.1 ml/h proved to be optimum to achieve a steady nanofibre morphology. It was thus concluded that to achieve a bead-free, uniform and smooth nanofibres that could likely be ideal for CO₂ capture, a combination of feed solution greater or equal to 18 % wt./vol., the feed flow rate at 1 ml/h and TCD between 10 and 12 cm will be sufficient at a voltage of 20 kV or less.

References

- Abdul Hameed, M. M., Mohamed Khan, S. A. P., Thamer, B. M., Rajkumar, N., El-Hamshary, H. and El-Newehy, M. (2023). Electrospun nanofibres for drug delivery applications: Methods and mechanism. *Polymers for Advanced Technologies*, 34(1): 6-23.
- Bhardwaj, N. and Kundu, S. C. (2010). Electrospinning: A fascinating fibre fabrication technique. *Biotechnology advances*, 28(3): 325-347.
- Contreras-Cáceres, R., Cabeza, L., Perazzoli, G., Díaz, A., López-Romero, J. M., Melguizo, C. and Prados, J. (2019). Electrospun nanofibres: Recent applications in drug delivery and cancer therapy. *Nanomaterials*, 9(4): 656. doi: 10.3390/nano9040656
- Dos Santos, D. M., Correa, D. S., Medeiros, E. S., Oliveira, J. E. and Mattoso, L. H. (2020). Advances in functional polymer nanofibres: From spinning fabrication techniques to recent biomedical applications. *ACS applied materials and Interfaces*, 12(41): 45673-45701.
- Fayemiwo, K. A., Chiarasumran, N., Nabavi, S. A., Loponov, K. N., Manovic, V., Benyahia, B. and Vladislavljevic, G. T. (2019). Eco-friendly fabrication of a highly selective amide-based polymer for CO₂ capture. *Industrial and Engineering Chemistry Research*, 58(39): 18160-18167.
- Fayemiwo, K. A., Vladislavljević, G. T., Nabavi, S. A., Benyahia, B., Hanak, D. P., Loponov, K. N. and Manović, V. (2018). Nitrogen-rich hyper-crosslinked polymers for low-pressure CO₂ capture. *Chemical Engineering Journal*, 334: 2004-2013.
- Feng, C., Khulbe, K. C. and Matsuura, T. (2010). Recent progress in the preparation, characterization, and applications of nanofibres and nanofibre membranes via electrospinning/interfacial polymerization. *Journal of Applied Polymer Science*, 115(2): 756-776.
- Gür, T. M. (2022). Carbon dioxide emissions, capture, storage and utilization: Review of materials, processes and technologies. *Progress in Energy and Combustion Science*, 89: 100965.
- He, Z., Rault, F., Lewandowski, M., Mohsenzadeh, E. and Salaün, F. (2021). Electrospun PVDF nanofibres for piezoelectric applications: A review of the influence of electrospinning parameters on the β phase and crystallinity enhancement. *Polymers*, 13(2): 174. doi: 10.3390/polym13020174.
- Iqbal, N., Wang, X., Yu, J. and Ding, B. (2017). Robust and flexible carbon nanofibres doped with amine-functionalized carbon nanotubes for efficient CO₂ capture. *Advanced Sustainable Systems*, 1(3-4): 1600028.

- Kumar, V., Naqvi, S. and Gopinath, P. (2018). Applications of nanofibres in tissue engineering. In *Applications of nanomaterials* (pp. 179-203). Woodhead Publishing.
- Lee, K. J., Shiratori, N., Lee, G. H., Miyawaki, J., Mochida, I., Yoon, S. H. and Jang, J. (2010). Activated carbon nanofibre produced from electrospun polyacrylonitrile nanofibre as a highly efficient formaldehyde adsorbent. *Carbon*, 48(15): 4248-4255.
- Li, Y., Zou, B., Hu, C. and Cao, M. (2016). Nitrogen-doped porous carbon nanofibre webs for efficient CO₂ capture and conversion. *Carbon*, 99: 79-89.
- Li, Y., Zou, B., Hu, C. and Cao, M. (2016). Nitrogen-doped porous carbon nanofibre webs for efficient CO₂ capture and conversion. *Carbon*, 99: 79-89.
- Long, Y. Z., Yu, M., Sun, B., Gu, C. Z. and Fan, Z. (2012). Recent advances in the large-scale assembly of semiconducting inorganic nanowires and nanofibres for electronics, sensors and photovoltaics. *Chemical Society Reviews*, 41(12): 4560-4580.
- Mac Dowell, N., Fennell, P. S., Shah, N. and Maitland, G. C. (2017). The role of CO₂ capture and utilization in mitigating climate change. *Nature climate change*, 7(4): 243-249.
- Malik, S., Sundarrajan, S., Hussain, T., Nazir, A., Ayyoob, M., Berto, F. and Ramakrishna, S. (2021). Sustainable nanofibres in tissue engineering and biomedical applications. *Material Design and Processing Communications*, <https://doi.org/10.1002/mdp2.202>
- Min, L. L., Zhong, L. B., Zheng, Y. M., Liu, Q., Yuan, Z. H. and Yang, L. M. (2016). Functionalized chitosan electrospun nanofibre for effective removal of trace arsenate from water. *Scientific reports*, 6(1): 1-12.
- Ouyang, J., Gu, W., Zheng, C., Yang, H., Zhang, X., Jin, Y... and Jiang, J. (2018). Polyethyleneimine (PEI) loaded MgO-SiO₂ nanofibres from sepiolite minerals for reusable CO₂ capture/release applications. *Applied Clay Science*, 152: 267-275.
- Oyewole, K. A., Okedere, O. B., Rabiou, K. O., Alawode, K. O. and Oyelami, S. (2023). Carbon dioxide emission, mitigation and storage technologies pathways. *Sustainable Environment*, 9(1): 2188760.
- Schoolaert, E., Hoogenboom, R., and De Clerck, K. (2017). Colorimetric nanofibres as optical sensors. *Advanced Functional Materials*, 27(38): 1702646.
- Sing, K. S. (1985). Reporting physisorption data for gas/solid systems with special reference to the determination of surface area and porosity (Recommendations 1984). *Pure and applied chemistry*, 57(4), 603-619.
- Thompson, C. J., Chase, G. G., Yarin, A. L. and Reneker, D. H. (2007). Effects of parameters on nanofibre diameter determined from electrospinning model. *Polymer*, 48(23): 6913-6922.
- Wahiduzzaman, A., Khan, M., Absar, S., Harp, S., Edwards, K. and Takas, N. (2015). Fabrication of polyacrylonitrile nanofibre membranes functionalized with metal organic framework for CO₂ capturing. In *ASME International Mechanical Engineering Congress and Exposition* (Vol. 57526, p. V009T12A071). American Society of Mechanical Engineers.
- Xue, J., Xie, J., Liu, W. and Xia, Y. (2017). Electrospun nanofibres: new concepts, materials, and applications. *Accounts of chemical research*, 50(8): 1976-1987.